Cellular Snow Generation—A Doppler Radar Study[1]

R. E. CARBONE[2] AND ALAN R. BOHNE

Laboratory for Atmospheric Probing, University of Chicago and Illinois Institute of Technology, Chicago 60637

(Manuscript received 19 June 1974, in revised form 17 January 1975)

ABSTRACT

Snow generating cells were observed by vertically pointing Doppler radar. Analysis was carried out in three distinct regions. The region exhibiting cellular structure was found to consist of convective elements with vertical velocities ± 1.5 m s^{-1} in magnitude. A generation region was found to exist beneath the convective region with updrafts of 0.5 m s^{-1} sustained over a 7 km path length which originated at a generating level less than 75 m in depth associated with an inversion layer. The trail region below exhibited maximum downdrafts of 0.5 m s^{-1} or no net vertical motions.

Maximum ice content was estimated to be no larger than 0.24 g m^{-3} in the convective cells. Growth appeared to take place throughout the rise and fall of the snow crystals in the updraft regions.

1. Introduction

Snow generation in the middle and upper troposphere has been a topic of considerable investigation among cloud physicists and radar meteorologists during the past 20 years. The term "generating level" was introduced by Marshall (1953) to describe the region in which cells or heads provide the environment for the growth of ice crystals which subsequently produce trails of precipitation. Wexler (1955) deduced from radar observations that snow falls from cumuliform clouds based at the generating level. He found the cells to be circular, approximately 1 mi in diameter, oriented in bands, and located in the middle troposphere. He concluded that the ice crystals grow by both deposition and riming, and achieve terminal velocities of 1.0–1.5 m s^{-1}.

Langleben (1956) observed snow generators by incoherent scanning radar. He constructed constant altitude maps from PPI data and deduced that the convective cells had a lifetime of several hours and were 1–3 km in diameter and about 1 km deep. Langleben found the cells to move with the wind at the base of the cell, and defined this level as the generating level. The horizontal distribution of cells was pseudo-random in conditions of low wind shear with a tendency for the cells to form long lines when the vertical shear of the horizontal wind was larger.

Douglas *et al.* (1957) observed similar generating cells by vertically pointing radar and deduced that release of latent heat due to deposition was primarily responsible for the convective development. Douglas *et al.* also theorized that severe sublimational cooling takes place in a dry stable layer just below the generating level, thereby producing convective instability and long-lasting cells. They estimated updrafts in the cells to be 1.0–3.0 m s^{-1} on the basis of calculations which included latent heat and thermal stability considerations.

Wexler and Atlas (1959) attempted to put the phenomenon into synoptic context as well as to make a more quantitative analysis of cellular snow generation. They suggested that advection of dry air aloft, east of an upper air trough, produced convective instability in a thin layer—the generating level. Their radar observations first showed cells without trails, then trails without cellular heads. The cells had a maximum radar reflectivity factor Z of 23 dBZ located at the base of the cells.[3] They concluded that the crystal growth took place throughout its rise and fall within the cell. Estimates of updraft velocity were obtained by estimating the precipitation rate from the radar reflectivity factor and subsequently calculating a layer-averaged updraft which produces precipitation at that rate. They deduced updrafts varying from 0.20 to 1.1 m s^{-1}.

[1] Research supported by grants from the Office of Naval Research (N00014-67A-0285-0014) and the National Science Foundation (GA-38109).

[2] Present affiliation: Meteorology Research, Inc., Altadena, Calif. 91001.

[3] The radar reflectivity factor Z for particles small compared to the wavelength is defined as the sum of the sixth powers of the melted diameters of the particles contained in unit volume. This quantity is usually expressed in dimensions of mm^6 m^{-3} and 10 $\log_{10} Z$ is referred to as the dBZ value. Thus 23 dBZ is equivalent to a radar reflectivity factor of about 200 mm^6 m^{-3}.

Yagi (1969) observed cirrus generators by stereophotogrammetric methods. He found that the clouds developed in a dry adiabatic layer with vertical shear of the horizontal wind. In the case of cirrus uncinus, extremely stable layers existed above and below the cloud and the trail was generally confined to the stable layer.

Oddie (1959) observed small cumuliform clouds develop behind mature generating cells and above their trails. He concluded that such a region is favorable for horizontal convergence and thus leads to a succession of generating cells.

Heymsfield (1973) studied cirrus uncinus cells by aircraft measurements, laboratory experiments, and numerical modeling. His aircraft measurements found crystal concentrations of 10^5 m^{-3} and the average crystal size between 0.5 and 1.0 mm. Ice content (hereinafter IC) was calculated to be as large as 0.4 g m^{-3} in the uncinus cells and updrafts were calculated to be 1–2 m s^{-1} assuming mass flux continuity between the cloud head and trail. A numerical model showed that release of latent heat at -35°C did not significantly enhance updraft velocity. In addition, Heymsfield's observation of stable layers above and below the uncinus cells suggest that forced convection may be the sole mechanism initiating uncinus development at temperatures less than -30°C. Heymsfield also emphasized the potential role of convectively induced horizontal convergence in the presence of vertical shear and trail merging in the production of long-lasting cells.

From the above, it can be seen that our knowledge of the vertical air motion in snow generating cells is based on indirect estimates from conventional radar and aircraft measurements of precipitation rates and particle-size distributions. This study presents the distribution of vertical velocities in snow generators deduced from vertically pointing Doppler radar observations. In addition, a preliminary analysis of Doppler spectral properties at the base of the generation region is performed in an attempt to resolve the causes of convection initiation. The limitations inherent in determining three-dimensional flow fields and hydrometeor distributions from vertically pointing radar observations are also discussed.

2. The observations

The radar used for the observation is an FPS-74 S-band system with 1.0 μs pulse, 0.6° nominal beam width, and peak transmitted power of 1.0 MW. One component of the bipolar video signal was recorded on video tape, digitized, and spectrum-analyzed to obtain Doppler velocity spectra. To avoid ambiguities between positive and negative Doppler velocities, the bipolar video signal was shifted in frequency by one-fourth the pulse repetition frequency (974 Hz). The system permitted an unambiguous Doppler velocity range of approximately ± 12.5 m s^{-1}.

Vertically pointing Doppler radar measurements of precipitation were performed over Chicago during the afternoon of 13 November 1972. Precipitation echo was continuous throughout the period of observations from the surface to 3.0 km aloft. Cellular echoes emanated from 6 and 9 km heights intermittently throughout the period and the cells frequently exhibited the familiar precipitation trail structure below. A 15 min (1700–1715 CST) period was chosen for detailed analysis. Selection of this period was based on the well-defined reflectivity structure, quality of tape-recorded data, and proximity in time to available upper-air synoptic data.

The major features of the reflectivity pattern are shown in Fig. 1a which is a contoured time-height cross section of the reflectivity factor, the contour spacing being 3 dBZ. The quantitative reflectivity factors were determined from data recorded on magnetic tape. An equivalent space scale has been inserted based on an estimate of the mean upper winds at the time of observation. Maxima of reflectivity factor are seen to exist in the convective cells (marked by $\times$'s), in a thin layer at 5.2 km, and in the trail region below. Hereinafter the authors will refer to cells II and III which are the structures at 1708 and 1712, respectively. The trail structure between 1703 and 1709 suggests a cell at 1703 which may be outside the radar beam. This cell will be referred to as cell I. The largest reflectivity factor of 22 dBZ occurs within the trail associated with cell I. Maxima of 18 dBZ at the 5.2 km layer occur beneath cells II and III, which is similar to the structure observed by Wexler and Atlas (1959). Maxima of 16 and 17 dBZ are marked by $\times$'s within cells II and III, respectively.

Doppler velocity spectra were computed every 3 s at height intervals of 100–150 m for the 15 min period. Moments of the spectra were calculated and Fig. 1b is the resulting time-height cross section of mean Doppler velocity $\bar{v}_D$. Contours are given at 0.5 m s^{-1} intervals. The shaded areas in cell III indicate where $\bar{v}_D$ is upward —that is, where most, if not all, of the particles are being carried aloft. If, for the moment, we assume $\bar{v}_D = -1.0$ m s^{-1} as an approximation to the mean Doppler velocity in the absence of vertical air motion, then several important features of the motion field become evident. Updrafts of about 2 m s^{-1} are implied in the reflectivity core of cells II and III and compensating downdraft on the edge of the cells also appears to be present. There is a sharp gradient in $\bar{v}_D$ between 5.1 and 5.2 km which is coincident in time and space with the reflectivity maximum at that level. In addition, a downdraft is indicated just below the leading edge of the trail associated with cell I. It may be mentioned here that the lowest reflectivity factor contour displayed in Fig. 1a is 0 dBZ, although the minimum detectable Z for the radar at a range of 6 km is approximately -22 dBZ. Detectable signal was present in the region between cells II and III.

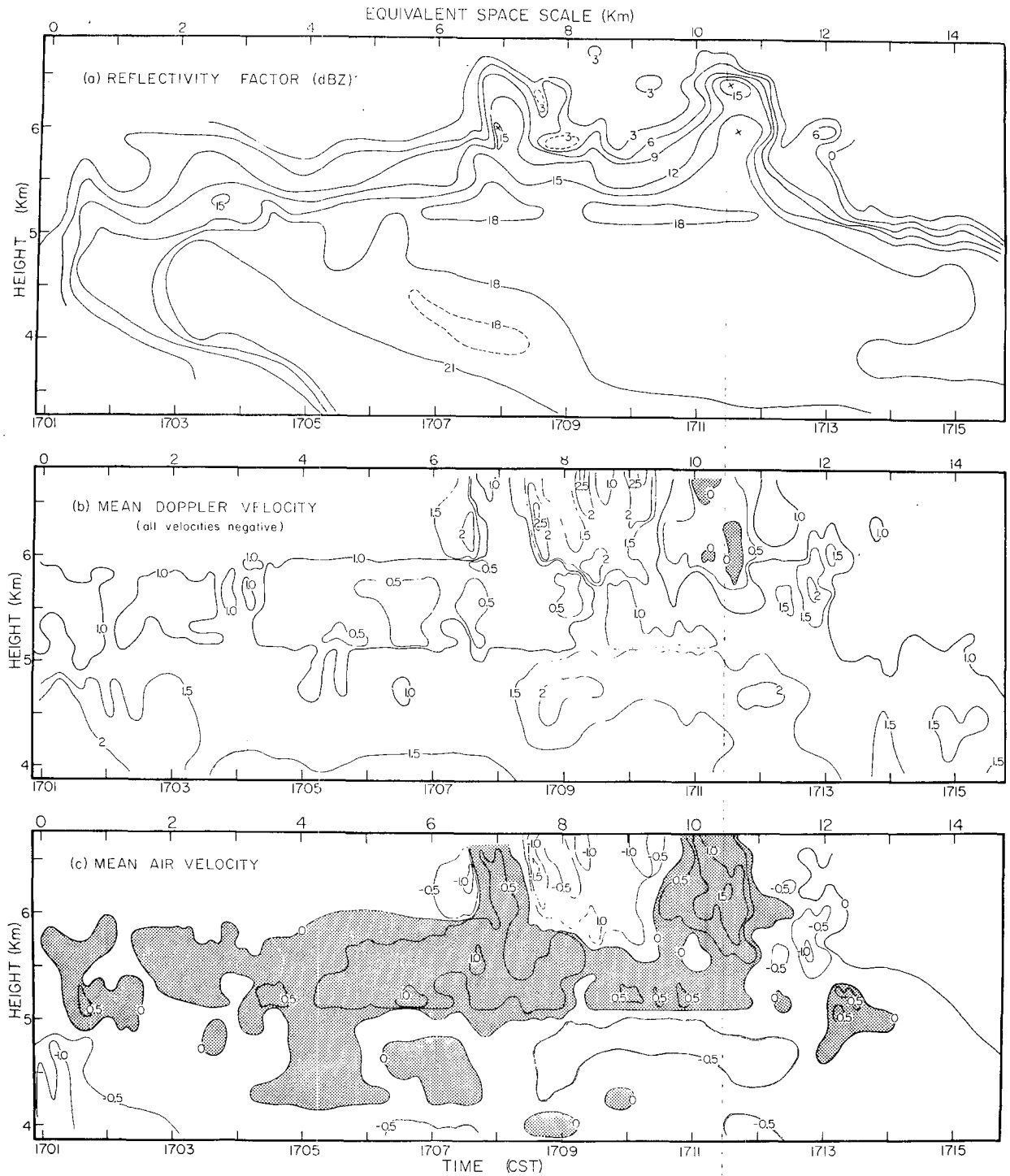

FIG. 1. Digitized time-height sections of (a) reflectivity factor, (b) mean Doppler velocity and (c) estimated mean air velocity. See text for explanation.

A clearer picture of vertical air motion may be obtained by the assumption of a relationship between mean, reflectivity-weighted, particle velocity $\bar{v}_P$ and the reflectivity factor Z. The correct choice of a $\bar{v}_P$-Z relationship is dependent upon the particle size distribution and the terminal velocity vs size dependence. A family of such relationships exists in the literature, some of which are more appropriately applied to single crystal snow and others to rimed crystals or aggregates. Several relationships of the form $\bar{v}_P = cZ^k$ were tested

on the data assuming an exponential form for the particle-size distribution:

$$N(D)=N_0 \exp[-\Lambda D], \quad (1)$$

where $N(D)$ is the number concentration per unit volume per unit size interval of particle diameter D. Use of such a $\bar{v}_P$-Z relation assumes an approximate fallspeed dependence of the form $v_P=aD^b$, where $k=b/7$ and $a=c(720N_0)^k/[\Gamma(7+b)/\Gamma(7)]$ as shown, for example, by Atlas *et al.* (1973). Since *in situ* measurements of crystal concentrations and characteristics were not available, it was decided that the best criterion for selection of a $\bar{v}_P$-Z relationship was zero vertical motion in the time-space domain under investigation. It should be remembered, however, that zero net vertical motion may not necessarily exist in the region containing the detectable scatterers. This criterion results in the equation

$$\bar{v}_P=0.92Z^{0.063} \quad (2)$$

at 500 mb, −20°C. When corrected for air density at 1000 mb and 0°C the implied fallspeed constants are

$$a=247 \text{ cm}^{(1-b)} \text{ s}^{-1} \quad \text{and} \quad b=0.44$$

for $N_0=0.79$ cm^{-4} given a total crystal concentration of 10^4 m^{-3} for a reflectivity factor of 15 dBZ. The crystal concentration was estimated based on aircraft measurements by Heymsfield and Knollenberg (1972) in cirrus from −15 to −30°C. These values of a and b differ significantly from the results of Langleben (1954) who found for aggregate snow that $a=207$ and $b=0.31$. This difference may largely be attributed to the fact that significant aggregation could not have taken place at −20°C, the particles consisting of single crystals with some unknown degree of riming.

The use of several other $\bar{v}_P$-Z relations resulted in the rather unlikely conclusion that the air was falling (or rising) over a 20 km path. Use of Eq. (2) in regions of aggregation ($h\leqslant 3$ km, $T\geqslant -10$°C) resulted in nearly uniform "downdrafts" during the entire time period. Therefore, Eq. (2) has been applied only to the data at heights >3 km.

Fig. 1c illustrates the deduced vertical air velocity field (m s^{-1}) where

$$\bar{v}_A=\bar{v}_D-\bar{v}_P.$$

The estimated $\bar{v}_A$ field supports the qualitative, non-Doppler radar observation of previous studies. Updraft in excess of 1.5 m s^{-1} exists in the high-reflectivity core of cell III. The maximum updraft in cell II is nearly 1.0 m s^{-1}. Compensating downdrafts in the low-reflectivity regions beside and between the updrafts commonly exceed 1.0 m s^{-1}. Little or no updraft appears to remain in the region which may have been the base of cell I. The strong correlation between reflectivity and updraft strengthens the observations of previous investigators that convection produces vertical motion allowing released water vapor to become available for particle growth. The low reflectivity factor in the downdraft regions between cells II and III suggests that most of the particles are falling back through the updraft rather than diverging aloft into the downdraft. The inclination of the isopleths in Fig. 1 suggests weak negative shear of the horizontal wind between 5.4 and 6.0 km and positive shear above (positive shear means wind speed increasing with height).

A second region of interest is the layer 5.0 to 5.3 km where there is a sharp gradient of vertical velocity under cells II and III. At 5.2 km updraft from 0.2 to 1.0 m s^{-1} exists for a 7 min (~7 km) period. At 5.0 km $\bar{v}_A$ is either near zero or negative. If Eq. (2) is valid in this region, the implication of strong horizontal convergence up to 10^{-2} s^{-1} is obvious. This layer is coincident with a layer of maximum Z equal to 18 dBZ at 5.2 km. Clearly, this is a region of extreme importance to the structure of the precipitation generation phenomena as a whole and will be discussed in greater detail in Section 4. This layer is called the generating level since it is the base of the updraft which evolves into cellular convection aloft.

Substantial downward air motion is present at the leading edge of the snow trail at 1701:30. The upper bound of this region is 4.8 km which is just below the base of the generating level. Heymsfield (1973) found such downdrafts in trails of cirrus uncinus and attributed them to the negative buoyancy introduced by particle loading.

The Peoria, Ill., 1800 CST sounding (Fig. 2) placed the generating level in the vicinity of a thin inversion layer at 5 km with a nearly dry adiabatic lapse rate immediately above. The Green Bay, Wisc., sounding showed an inversion structure similar to that of Peoria but 200 m higher. Divergent upper level winds were favorable for widespread lifting of 10–20 cm s^{-1} which could aid the initiation of convection. Upper level moisture availability appeared to be spotty at 500 mb which conforms to the observation of intermittent precipitation above 3 km.

3. Cellular convection

It is clear from Fig. 1 that maximum updraft and reflectivity factor are highly correlated and that convective release of excess water vapor permits precipitation growth. In order to verify the physical plausibility of a 1.0–1.5 m s^{-1} updraft producing a 17 dBZ echo within a 1.0 km vertical displacement, it is instructive to evaluate some simple equations. Douglas *et al.* (1957) have evaluated updraft production due to the release of latent heat in environmental lapse rates ranging from isothermal to moist adiabatic. Depending upon the thermal stability, their calculated updrafts ranged from 1.0 to 3.0 m s^{-1} at −15°C and 700 mb.

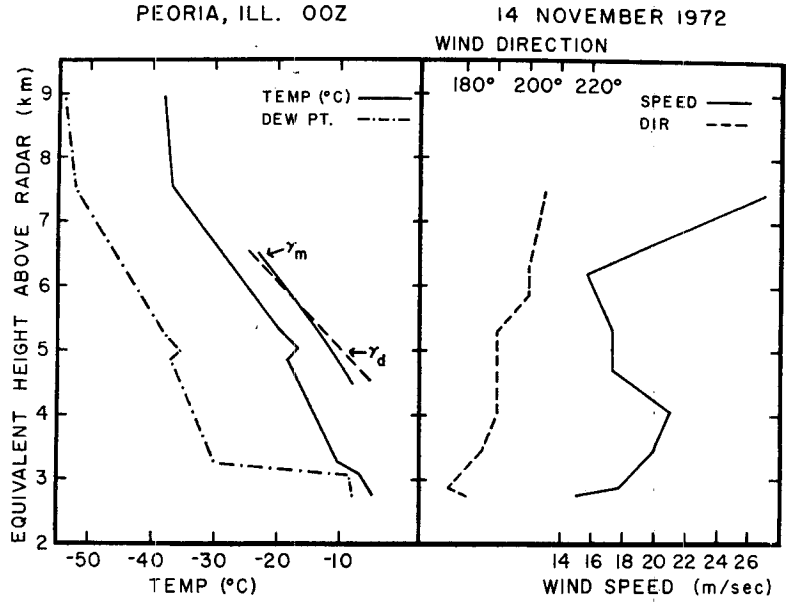

FIG. 2. Upper air conditions as given by Peoria sounding 200 km southwest of Chicago. Note the inversion at 5 km and the dry upper air conditions.

The following equation for the ice content (IC) results from Eq. (1) (see, for example, Atlas *et al.*, 1973):

$$\mathrm{IC}=\left(\frac{\pi\rho N_0}{\Lambda^4}\right)10^6\ [\mathrm{g\ m^{-3}}], \tag{3a}$$

where ρ is the density of water and N_0 and Λ are in $\mathrm{cm^{-4}}$ and $\mathrm{cm^{-1}}$, respectively. N_0 and Λ may be related to N_T and Z yielding

$$\mathrm{IC}=\pi\rho\left(\frac{ZN_T}{120}\right)^{\frac{1}{2}}10^{-3}\ [\mathrm{g\ m^{-3}}], \tag{3b}$$

where Z and N_T are in $\mathrm{mm^6\ m^{-3}}$ and $\mathrm{m^{-3}}$, respectively. The maximum reflectivity factor observed in the cellular region was 17 dBZ and N_T may vary between 5×10^3 and $5\times10^4\ \mathrm{m^{-3}}$ at -20°C as shown by the observations of Heymsfield and Knollenberg (1972). Substituting into Eq. (3b), IC is calculated to be within a factor of about 2 of 0.12 $\mathrm{g\ m^{-3}}$ depending on the selection of N_T. It can be shown that a parcel ascending moist adiabatically and conserving water substance, will achieve a total water content of 0.2 $\mathrm{g\ m^{-3}}$ in less than 400 m centered at -20°C and 500 mb.

Similar calculations may be performed in order to assess the effect of particle loading and latent heat on the updraft through use of the following equations:

$$\Delta T=\frac{(L_s-L_v)M}{\rho_a c_P}, \tag{4}$$

$$\frac{dw}{dt}=w\frac{dw}{dz}=g\left(\frac{\Delta T}{T}-\frac{M}{\rho_a}\right), \tag{5}$$

where ΔT is temperature excess, L_s and L_v are latent heat of sublimation and vaporization (cal $\mathrm{g^{-1}}$), respectively, M is water content ($\mathrm{g\ m^{-3}}$), c_P the specific heat of air (cal $\mathrm{g^{-1}\ K^{-1}}$) and ρ_a air density ($\mathrm{g\ m^{-3}}$). Eq. (4) represents the smallest possible contribution of latent heat where ice crystals are grown by deposition in a moist adiabatic environmental lapse rate so that only the latent heat of fusion ($\sim$70 cal $\mathrm{g^{-1}}$) is realized as a temperature excess. Substituting Eq. (4) into Eq. (5) and integrating, it follows that

$$w^2-w_0^2=\frac{2g}{\bar{\rho}_a}\left(\frac{L_f}{c_P\bar{T}}-1\right)\int_{z_0}^{z}M(z)dz, \tag{6}$$

where $\bar{\rho}_a$, $\bar{T}$ are taken as constant over the layer and M is a function of the height. The production of water vapor in excess of saturation with respect to water may be approximated by

$$M(z)=kz,$$

where $k=5\times10^{-4}\ \mathrm{g\ m^{-4}}$ at -20°C and 500 mb. Eq. (6) now becomes

$$w^2-w_0^2\approx10^{-6}\Delta z^2\ [\mathrm{s^{-2}}].$$

If $w_0=0$ and $\Delta z=1$ km, then an updraft of 1 $\mathrm{m\ s^{-1}}$ results for the snow generation situation. Clearly, if either the environmental lapse rate is slightly destabilized with respect to moist adiabatic or precipitation is allowed to fall out of the parcel, larger updrafts will result. Moreover, the parcel may not remain at water saturation during its ascent, in which case the latent heat contribution will increase significantly and further enhance the updraft. Thus, it can be seen that conservative estimates

are capable of generating updrafts of the magnitude seen in the radar data.

It will now be shown that the excess water vapor made available in a 1 m s^{-1} updraft can be consumed by pure deposition without the water phase playing any dominant role in the latent heat exchange. The rate of deposition on an ice crystal is given by[4] (for example, Fletcher, 1966)

$$\left.\frac{dM}{dt}\right|_{\text{dep}} = 4\pi CGS_i, \tag{7}$$

where

$$G = D\rho_v\left(1+\frac{DL^2\rho_v M_0}{RT^2\kappa}\right)^{-1}.$$

The excess water vapor production rate E, resulting from an updraft w, is given by

$$E = \frac{c_P}{L}(\gamma_d - \gamma_m)w\rho_a, \tag{8}$$

where γ_d is the dry adiabatic lapse rate. The critical number concentration which can just consume water vapor at the rate E is given by

$$E = N_c\left.\frac{dM}{dt}\right|_{\text{dep}} = 6\times10^{-10}\ \text{g s}^{-1}\ \text{cm}^{-3},$$

where the right-hand side of the above equation has been evaluated according to Eq. (8) for $w=1$ m s^{-1}. Now since

$$\left.\frac{dM}{dt}\right|_{\text{dep}} = 1.5\times10^{-8}\ \text{g s}^{-1}$$

for a plate crystal of diameter 0.5 mm, we have

$$N_c = 4\times10^4\ \text{m}^{-3}.$$

If the actual crystal concentration exceeds N_c, the excess water vapor can be consumed by pure deposition. The above value of N_c is within the range of values measured by Heymsfield and Knollenberg (1972).

The above calculations are of little more than order of magnitude significance. Nevertheless, a consistency has been demonstrated to exist between measured radar reflectivity, Doppler velocity, buoyancy considerations, growth rate calculations, and the simple thermal bubble model of convection. Visual observations of cirrus generators by Heymsfield (1973) and others indicate that a typical lifetime of a cell is 20–30 min which corresponds to the total rise time of such a bubble. The authors are of the opinion that cells II and III in the data are the result of simple convective thermals between 5.6 and 7.0 km. The calculations given are conservative by two standards. First, the contribution of latent heat has been minimized by essentially using only the heat due to fusion as the source of buoyancy. Second, the environment has been assumed to be moist adiabatic when the Peoria sounding indicates a 300 m dry adiabatic layer at 5.3 km and Heymsfield (1973) has consistently observed a dry adiabatic lapse rate in cirrus uncinus.

The discussion to this point has centered on the characteristics of cells II and III and a question has been raised as to whether cell I exists outside the 70 m wide radar beam. Several previous investigators have suggested mechanisms such as sublimationally induced convection, natural convergence due to wind shear, and ice crystal seeding from aloft, as methods by which a temporal succession of cells can occur. Fig. 1 is highly suggestive of a temporal succession of cells. The well-defined trail appears to have emanated from a previously existent cell I. The growth cycle has been completed and $Z=22$ dBZ is the largest reflectivity factor in the time-height section. Moreover, cell III contains a more vigorous updraft field with maximum speed of 1.5 m s^{-1} compared to the "older" cell II with maximum updraft of 1.0 m s^{-1}. Cell II also contains a more vigorous downdraft than cell III, with maxima exceeding 2 m s^{-1}. This factor may be due to the effect of particle loading overcoming the positively buoyant factors.

There is another plausible argument, however, which explains these characteristics of the time-height section. Fig. 3 is a schematic representation of three cells which

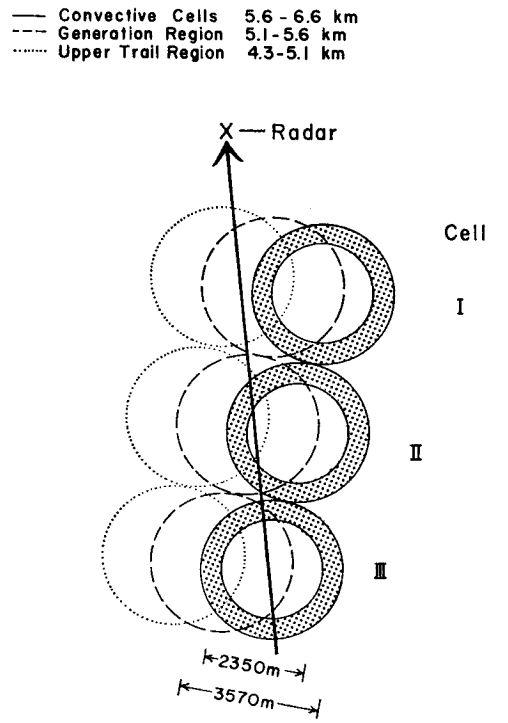

FIG. 3. Possible cell-trail configuration given 10°–15° of directional wind shear. Circles indicate cell heads, generation region and trails as they are displaced from path over radar beam.

[4] See the Appendix for definition of symbols.

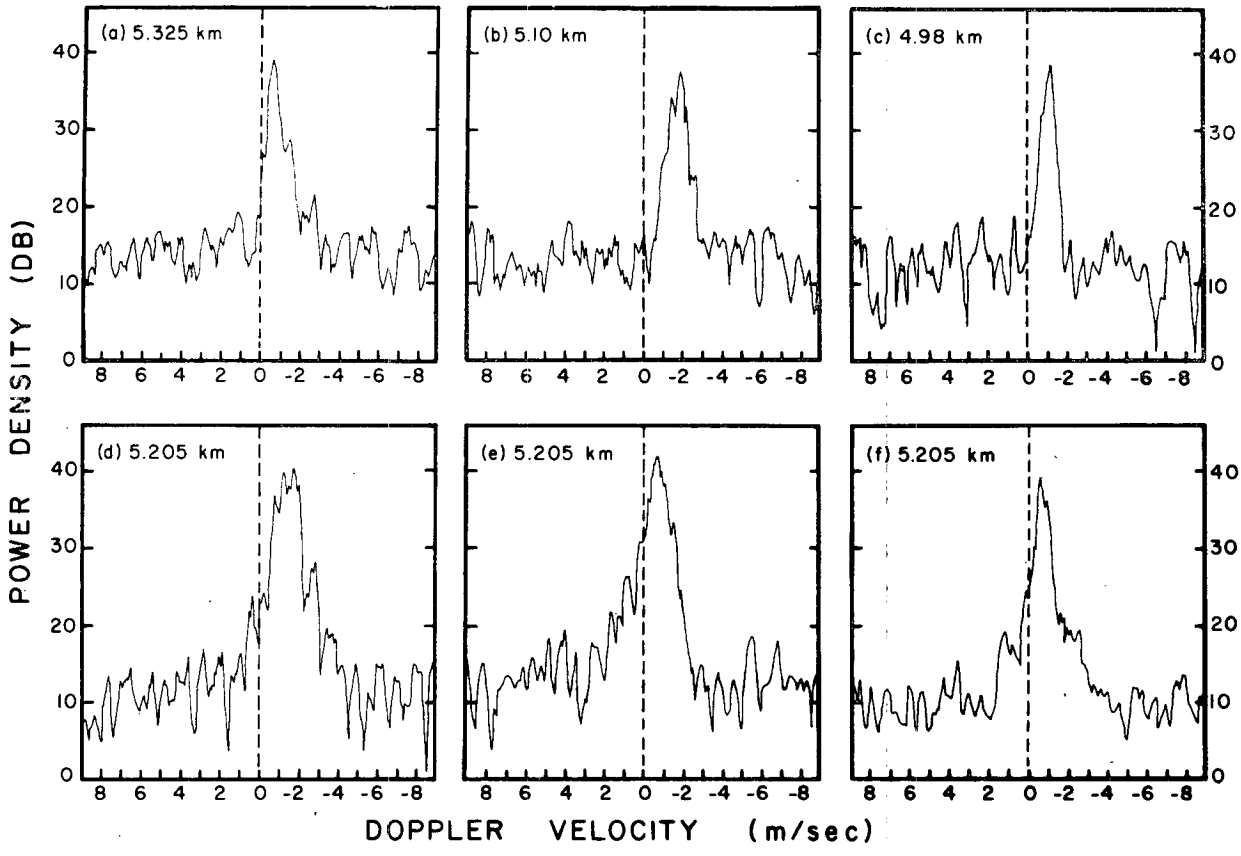

FIG. 4. Typical Doppler spectra from the generation level at 5.325 km (a), 5.10 km (b), 4.98 km (c), and at 5.205 km [(d), (e), (f)] where severe broadening near noise level takes place.

are oriented approximately 12° off the direction of translation. This configuration of cells is quite similar to that observed by Langleben (1956). The dark solid line indicates the path of translation over the radar beam. Three heights are shown, which depict the cellular convection from 5.6 to 6.6 km (solid), the generation region from 5.1 to 4.6 km (dashed), and the upper trail region below 5.1 km (dotted). The areas of updraft and downdraft (stippled) are equalized, thereby providing continuity for vertical motions of equal magnitude. The lateral displacement results from 12° of angular shear of the environmental winds between 6.5 and 4.5 km, which is consistent with the Peoria sounding. The precipitation is assumed to fall at ~ 1 m s^{-1}. Magnitude shear of the environmental wind is assumed to be negligible, although this assumption is not critical to the argument.

It is clear from Fig. 3 that the radar will see the strongest updraft in cell III and a weaker updraft in cell II which is surrounded by a large region of downdraft. Furthermore, cell I will not appear in the time-height section at the level of cellular convection; however, the trail of cell I will be centered in the beam. It is also obvious that maximum vertical velocity and reflectivity structure between 5.2 and 5.6 km will appear beneath cell II. Although Fig. 3 is merely a schematic representation, it is entirely consistent with the known facts and must be considered as an alternative to the temporal succession argument given previously. The question can only be resolved through simultaneous use of scanning and vertically pointing radar.

The authors have considered the region of cellular convection in some detail. What remains is to investigate the role of the generating level which appears to be the origin of free convection aloft.

4. The generating level

It can be seen from Fig. 1 that there is a layer of sharp transition of vertical velocity and reflectivity factor near 5 km. This region was chosen for detailed analysis because it is clearly the base of the updraft which evolves into cellular convection aloft. The region includes the transition from thermal inversion to (at least) conditional instability as indicated by the Peoria sounding. The sharp horizontal stratification of mean Doppler velocity and reflectivity over several kilometers indicates the presence of organized motions and convection. The objective here is to investigate this region in

order to determine the nature of the convection to the extent that the data permit.

The primary method of investigation is analysis of individual and layer-averaged properties of the Doppler velocity spectra. Doppler spectra were obtained at four levels in the region of interest, namely at 4.980, 5.100, 5.205 and 5.325 km above the radar. Successive spectra are separated by 3 s intervals and the analysis has been performed over a 7 min period (1705–1712) centered on the region below cells II and III. This time period was chosen in view of the discussion relating to Fig. 3 and the relative homogeneity of the data levels throughout the period. Fig. 4 illustrates typical Doppler power spectra for each of the data levels. The ordinate is a logarithmic scale of power density and the abscissa vertical velocity (m s^{-1}). The computation of spectral moments and the determination of bounds are performed based on the threshold which is typically 15 to 25 dB below the peak of the Doppler spectrum and just above the peak noise level, which was determined by the technique suggested by Hildebrand and Sekhon (1974).

Figs. 4a, b and c are typical spectra from the 5.3, 5.1 and 4.98 km levels, respectively. It can be seen that the spectrum at 5.3 km is shifted slightly toward the left (updraft) relative to those in 4b and 4c. The spectra at 5.1 and 4.98 km are skewed slightly toward the left and at 5.3 km the spectrum is skewed toward the right. The spectra at all three levels are relatively narrow with bound-to-bound width of approximately 2 m s^{-1} and standard deviation σ_v of 0.2–0.3 m s^{-1}. Occasionally spectra at these levels exhibit well-defined multiple peaks and bound-to-bound width as large as 3 m s^{-1}.

Figs. 4d, e and f are sample spectra from the 5.2 km level. Here the spectral characteristics are significantly different from the levels above and below. They commonly exhibit multiple peaks (4d), pronounced skewness (4e) and relatively broad bounds.

The obvious difference between the Doppler spectra at 5.2 km and the surrounding levels indicates that some physical process is taking place within a thin layer which is less than the 150 m pulse depth. The 5.2 km level is the lowest level at which updraft occurs. Therefore, information as to the physical mechanism(s) responsible for initiation of convection should be present within this region.

Properties of the individual and layer-averaged Doppler spectra provide information as to air motions on a sub-pulse volume scale (<150 m). Systematic differences in layer-averaged spectral properties should provide information on air motions with a scale (>100 m) larger than the pulse volume dimensions. Statistics were calculated from the spectra at each of the four levels by averaging spectral properties over the 7 min period. Layer-averaged quantities will be denoted by angular brackets $\langle\ \rangle$. Individual spectrum averages will continue to be shown by the overbar as in $\bar{v}_D$. It is important to note that information at each level is not completely independent of that obtained at adjacent levels since the range resolution is 150 m and the level separation is 100 to 130 m.

TABLE 1. Layer-averaged mean velocity and bounds.

Height	$\langle\bar{v}_D\rangle$ (m s^{-1})	$\langle LB\rangle$ (m s^{-1})	$\langle UB\rangle$ (m s^{-1})
4.98	−1.42	−0.55	−2.38
5.10	−1.26	−0.42	−2.20
5.205	−0.70	+0.26	−1.83
5.325	−0.78	+0.20	−2.0

The following layer-averaged spectrum quantities were computed:

1. $\langle\bar{v}_D\rangle$: average mean Doppler velocity
2. $\sigma_{\bar{v}D}=(\langle\bar{v}_D{}^2\rangle-\langle\bar{v}_D\rangle^2)^{\frac{1}{2}}$: standard deviation of $\bar{v}_D$ over the layer
3. $\langle UB\rangle$: average spectrum upper bound
4. $\langle LB\rangle$: average spectrum lower bound
5. σ_{UB}, σ_{LB}: standard deviation of each bound
6. $\langle UB-LB\rangle=\langle UB\rangle-\langle LB\rangle$: average bound-to-bound spectrum width
7. $[(\langle UB\rangle-\langle\bar{v}_D\rangle)-(\langle\bar{v}_D\rangle-\langle LB\rangle)]$: a measure of skewness.

Table 1 shows $\langle\bar{v}_D\rangle$, $\langle UB\rangle$ and $\langle LB\rangle$ at the four levels between 4.98 and 5.325 km. The sharp transition of vertical velocity between 5.1 and 5.2 km is obvious, averaging 0.56 m s^{-1}. The true gradient of $\bar{v}_D$ in this region must in fact be greater than this value because of pulse volume averaging over 150 m in height and the 45 m of common volume between the two measurement levels. $\langle\bar{v}_D\rangle_{5.2}$ is −0.7 m s^{-1} in a region of 18 dBZ where $\bar{v}_P$ probably exceeds −1.0 m s^{-1}. $\langle\bar{v}_D\rangle$ decreases slightly to −0.78 at 5.3 km. The lower bound represents the smallest fall velocities of the smallest ice crystals which are detectable by the radar. Since $\langle LB\rangle$ is +0.20 and +0.26 m s^{-1} at 5.3 and 5.2 km, respectively, many of the smaller ice crystals are rising in the updraft. A calculation has been performed in order to estimate the terminal velocity of the smallest detectable ice crystal. The minimum detectable concentration number density $N_{\min}(D)$ is given by

$$N_{\min}(D)=\frac{z'_{\min}}{D^6}\frac{dv}{dD},$$

where D is equivalent melted diameter and $Z'_{\min}$ the minimum detectable reflectivity factor divided by the unambiguous velocity interval of the radar. A conservative estimate of $N(D)$ is 3×10^{-3} cm^{-4} for particles of melted diameter 0.1 cm. It follows from the calculations that plates or columns from 0.3 to 0.5 mm length with terminal velocities of 0.3 to 0.6 m s^{-1} are marginally detectable. Crystals 0.6–0.8 mm in length with fall velocities 0.5 to 0.8 m s^{-1} are definitely detectable provided the assumed $N(D)$ is correct within an order of magnitude. Therefore $\langle LB\rangle=0.25$ m s^{-1}

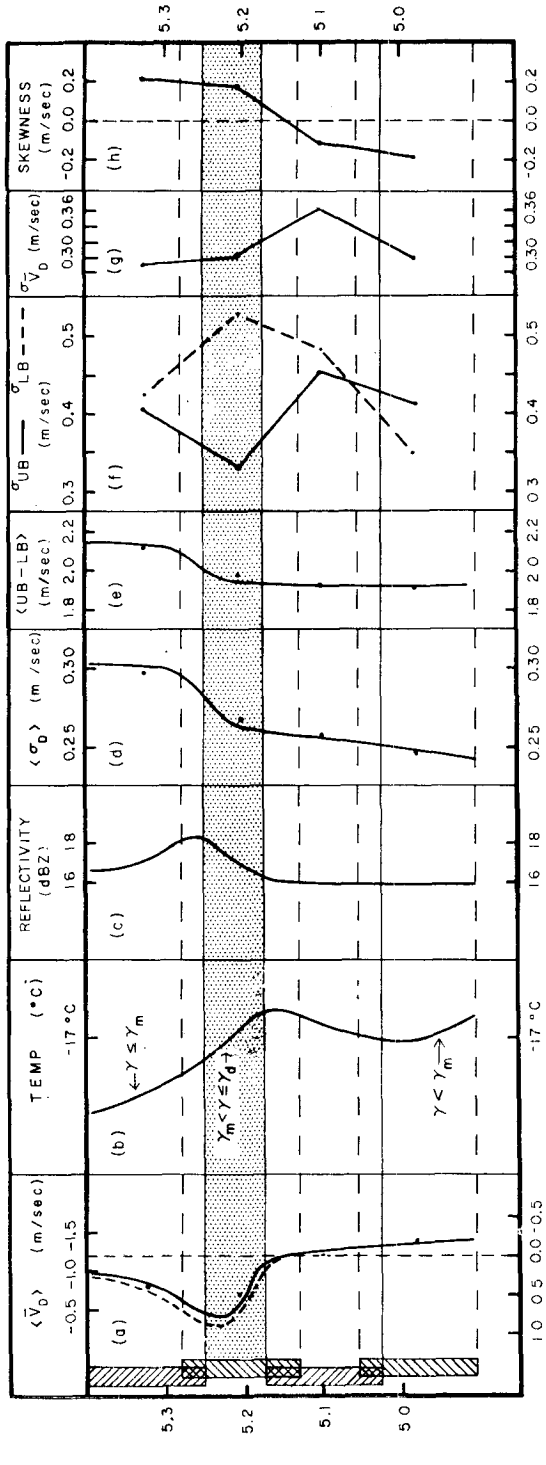

FIG. 5. Layer-averaged properties of the generating level with graphical deconvolution of selected quantities. See text for explanation. The lower abscissa in 5a is $\langle v_A \rangle$ (dashed line), also in units of m s^{-1}.

would suggest updraft in at least part of the pulse volumes to be of the order of 0.75 m s^{-1} at 5.2 and 5.3 km. This result is consistent with Eq. (3) and Fig. 1c.

Fig. 5 gives the layer-averaged Doppler spectrum properties, the reflectivity factor profile, and the deduced air velocity profile. Graphical deconvolution in height of certain quantities has been attempted in order to reveal the distribution of each quantity that would be measured by a radar with an infinitely narrow pulse. The deconvolution represents a best guess as to the actual physical situation. The original data points are shown with the interpolated curves. The cross-hatched sections at the left end of the figure represent the range resolution of the radar and the stippled region centered near 5.2 km extending through the entire figure represents that region common only to the pulse volume centered at 5.2 km.

Fig. 5a shows $\langle \bar{v}_D \rangle$ as a function of height. The computed values are shown as the four data points and the estimated smooth profile as the solid line. The air velocity, $\langle \bar{v}_A \rangle$, is shown by the dashed line on a translated scale where $\langle \bar{v}_A \rangle = 0$ when $\langle \bar{v}_D \rangle = 1.16$ m s^{-1}. This velocity translation results from application of Eq. (2) at 16 dBZ. $\langle \bar{v}_A \rangle$ goes from zero to 0.85 m s^{-1} updraft from 5.14 to 5.23 km height. This may be considered, for the moment, as vertical divergence of $\sim 10^{-2}$ s^{-1} which establishes an upper limit of compensating horizontal convergence necessary to maintain continuity. Such a convergence value is comparable to that which may occur in a convective storm and its validity must be questioned. One mechanism for reducing the apparent magnitude of convergence is to assume layer overrunning in a frontal zone. This could account for as much as 0.20 m s^{-1} vertical velocity on a mesosynoptic scale and thus decrease the convergence by 25%. There is synoptic evidence for an upper air front and a thermal structure to support this contention, i.e., an inversion at 5 km. However, overrunning can only take place if there is considerable vertical shear of the horizontal wind. There is no evidence of sufficiently large shear between 4.5 and 6 km in the available soundings. Consequently, the authors conclude that the major factor compensating the deduced vertical stretching is horizontal convergence 5×10^{-3} to 10^{-2} s^{-1} in magnitude over a 7 km path.

Fig. 5b is a schematic representation of the deduced temperature profile at the generating level. The profile is quite similar to that measured by the Peoria sounding. However, the inversion height has been raised by 100 m. In view of the fact that the sounding location is 200 km from the radar this is not an unreasonable adjustment, especially in the context of the radar data in Fig. 5. The temperature in the inversion layer is between −16 and −17°C. There is an unstable ($\gamma_d \geqslant \gamma \geqslant \gamma_m$) layer immediately above, and either a neutral or slightly stable layer ($\gamma \leqslant \gamma_m$) above it. The inversion is 120–180 m deep with a slightly stable layer

below. From Figs. 5a and 5b it can be seen that the updraft originates at the top of the inversion and increases in magnitude to its peak value of 0.85 m s^{-1} some 100 m above where thermal instability begins to decrease.

Fig. 5c is a schematic representation of the reflectivity factor profile. There is a sharp maximum (>18 dBZ) at 5.27 km which is just above the peak updraft in a region of apparently decreasing vertical air velocity. As the inversion top region is approached from above, the mean Doppler velocity is seen to decrease. Such a region may be favorable for particle accumulation as shown by

$$NV_D = N'V_D',$$

where N and N' are the initial and final equivalent particle concentrations which fall with the initial and final mean Doppler velocities V_D and V_D', respectively. Accumulation, however, does not necessarily take place since horizontal divergence may compensate fully. Furthermore, accumulation is not necessary to explain the reflectivity maximum, since precipitation falling from the cellular convection region aloft most probably is experiencing continuous growth by deposition during its fall. Rapid growth, primarily by deposition but also by riming, may take place in the generating level updraft, thereby producing the reflectivity maximum. If crystal lengths increase by 10%, Z increases by 3 dBZ. Since the maximum Z here is 1.0 to 2.0 dBZ above surrounding levels, the growth required is modest. While no new ice nucleation is required at this level, some nucleation probably takes place.

Reflectivity factor decreases sharply immediately below the updraft maximum. There is vertical stretching in this region which implies reduction in total particle concentration and a corresponding decrease in Z. Here one can be somewhat more confident that the particle number concentration is decreasing, since the horizontal convergence at this level is likely to be from a region which is relatively free of precipitation. Z should remain nearly constant below the inversion top, since there is no updraft to increase vapor density above ice saturation. It is possible, however, to have sublimation within the inversion layer which can ultimately generate convective instability and (at least temporarily) decrease Z. This process has either been measured or deduced by previous investigators as mentioned in the Introduction.

A sustained average maximum updraft of 0.85 m s^{-1} over a 7 km path suggests that particle size sorting takes place at and above the level of maximum updraft. We have shown earlier that the minimum detectable particle terminal velocity is between 0.4 and 0.7 m s^{-1}. If sorting of the smallest particles takes place then it should manifest itself as a decrease in the variance and particularly in the bound-to-bound width of the Doppler spectrum. Caution must be taken at this point because there are several well-known factors which affect the width of the Doppler spectrum. However, considering all other factors equal, $\langle UB-LB\rangle$ should decrease downward to the height of the peak updraft. This result is shown in Fig. 5e where the decrease is 0.2 m s^{-1}. This implies that the minimum detectable particle terminal velocity is 0.65 m s^{-1} which is consistent with the earlier calculations. It should be pointed out that the statistical significance of $\langle UB-LB\rangle$ is low given that the variance of this quantity is 0.16 m^2 s^{-2}. Fig. 5d shows a corresponding decrease of 0.03 m s^{-1} in the spectrum standard deviation below the updraft maximum.

It was shown in Fig. 4 that the Doppler spectra with the largest bound-to-bound widths were at 5.2 km where the strong gradient of vertical air motion exists. This observation is not apparent from Figs. 5d and 5e due to the peak-noise thresholding technique. The spectral broadening is apparent from spectral densities which are between peak- and average-noise levels, indicating that the extreme velocity values were quite limited in their spatial extent. The fluctuation of the spectral bounds have been calculated and are shown in Fig. 5f. The only statistically significant (>90%) feature is the fact that $\sigma_{LB} \geqslant \sigma_{UB}$ at 5.2 km. This is consistent with the unstable thermal structure in the upper part of the pulse volume and the stable structure in the lower part. The primary region of spectral broadening is believed to lie in a thin layer at the inversion top. The lower bound is representative of the smallest ice particles which are found at and above the unstable inversion top and are moving upward. Here, upward perturbations will experience positive buoyancy and amplification resulting in an increased σ_{LB}. The upper bound is representative of the largest particles with the greatest fallspeeds which are located in the stable region below the inversion top. Here downward perturbations will be damped resulting in a decreased σ_{UB}. This is, perhaps, the most convincing argument for a severe spectrum broadening process existing in a thin layer at the inversion top.

Similarly, the inverse stability situation exists at the inversion base and Fig. 5f shows $\sigma_{LB} < \sigma_{UB}$. The reversal however has low statistical significance which may be due to the slightly stable lapse rate below the inversion.

Fig. 5g illustrates the standard deviation of $\bar{v}_D$ which has a small maximum at the 5.1 km level. One possible explanation for this is the fact that the upper edge of the pulse volume is at the inversion top. A slight fluctuation (in and out of the volume) in the height of the inversion top would cause a larger standard deviation at 5.1 km than at any other level.

Fig. 5h depicts a measure of skewness. The effect is small and results from a combination of stability criteria and particle-size sorting. Atlas *et al.* (1973) calculated snow fallspeed spectra to be skewed negatively due to reflectivity-factor weighting of the larger particles. Accumulation and nucleation of small crystals

above the updraft maximum combined with nonuniform vertical acceleration can reverse the skewness as indicated by Fig. 5h.

Throughout the analysis the authors have deduced the existence of various processes which directly modify the particle-size distribution. The conclusions drawn are based on the validity of Eq. (2) which is itself dependent on the particle-size distribution and are therefore open to question. Perhaps the most severe effect may result from particle-size sorting in the region around the peak updraft at the generating level. Calculations were performed assuming that all crystals up to 0.7 mm length are sorted out of the region below, thus truncating the exponential distribution. It was found that the reflectivity factor decreases by 1% and $\bar{v}_D$ increases by 0.25%, both of which are considered negligible. Similarly, crystals of up to 0.7 mm in length were assumed to exist in concentrations one order of magnitude larger than that implied by Eq. (1). The result is a 10% increase in Z and a 1.9% decrease in $\bar{v}_D$ over that of Eq. (2) for any given reflectivity factor. It follows that relative uncertainty in vertical air velocity between regions of extreme excess and deficit of small crystals is $\sim$0.03 m s^{-1} which is considered negligible for the purposes of this study.

5. Conclusions

Cellular convection has been shown to be responsible for snow generation in the case studied. Vertical velocities were measured to be $\pm$1.5 m s^{-1} with reflectivity maxima located in the updraft core. Maximum ice content was estimated to be 0.24 g m^{-3}. A detailed, but somewhat qualitative, analysis of the generating level leads to the tentative result that perturbations at the top of an inversion layer exist on a vertical scale $\leqslant$75 m and over a path at least 7 km long. This layer appears to be the source of what evolves into cellular convection aloft. The nature of the perturbations was not resolved; however, waves, turbulence and mesosynoptic-scale layer overrunning are considered to be the most likely mechanisms. The major characteristics of the generators are similar to those deduced by previous investigators.

Future research should include simultaneous use of scanning and vertically pointing Doppler radar to deduce the horizontal wind field and trail geometry. A spectrum analysis of $\bar{v}$ and Z may help to determine the presence of waves and/or turbulence. Radiosondes in and/or near the generators should be launched in order to provide accurate temperature and moisture profiles. Simultaneous aircraft measurements of particle-size spectra and type would complete the microphysical picture.

Acknowledgments. Thanks are due to Prof. R. C. Srivastava and Messrs. F. Ian Harris, Andrew Heymsfield and Peter Hildebrand for their stimulating discussions; to Helen Supert for typing and editing of the manuscript; and to Kazuya Fujita and Claudia Jacobson for drafting of the figures.

Acknowledgment is also made to the National Center for Atmospheric Research, which is sponsored by the National Science Foundation, for the computing time used in this research.

APPENDIX

List of Symbols

C	electrostatic capacitance (rate factor)
S_i	supersaturation relative to a plane ice surface
D	diffusivity of water vapor in air
ρ_v	saturation density of water vapor
L	latent heat of deposition
M_0	molecular weight of water vapor
R	universal gas constant
T	temperature
κ	conductivity of air
G	of Eq. (7) has been corrected from that given by Fletcher (1966) by a factor of $1/\rho_s$ where ρ_s is the density of ice.

REFERENCES

Atlas, D., R. C. Srivastava and R. S. Sekhon, 1973: Doppler radar characteristics of precipitation at vertical incidence. *Rev. Geophys. Space Phys.*, **11**, 1–35.

Donaldson, R. J., Jr., G. M. Armstrong, K. J. Banis and R. M. Dyer, 1972: Measurement of wind gradients in convective storms by Doppler radar. *Preprints 15th Radar Meteorology Conference*, Urbana, Ill., Amer. Meteor. Soc., 22–26.

Douglas, R. H., K. L. S. Gunn and J. S. Marshall, 1957: Pattern in the vertical of snow generation. *J. Meteor.*, **14**, 95–114.

Fletcher, N. H., 1966: *The Physics of Rainclouds*. Cambridge University Press, 389 pp.

Harris, F. I., and G. Heymsfield, 1972: Radar observations of intense undulance in an evaporating cloud layer. *Preprints 15th Radar Meteorology Conference*, Urbana, Ill., Amer. Meteor. Soc., 303–308.

Heymsfield, A. J., 1972: Ice crystal terminal velocities. *J. Atmos. Sci.*, **29**, 1348–1357.

——, 1973: A detailed study of the cirrus generating cell and the evolution of cirriform clouds. Ph.D. dissertation, The University of Chicago, 119 pp.

——, and R. G. Knollenberg, 1972: Properties of cirrus generating cells. *J. Atmos. Sci.*, **129**, 1358–1366.

Hildebrand, P., and R. S. Sekhon, 1974: Objective determination of the noise level in Doppler spectra. *J. Appl. Meteor.*, **13**, 808–811.

Langleben, M. P., 1954: The terminal velocity of snow aggregates. *Quart. J. Roy. Meteor. Soc.*, **80**, 174–181.

——, 1956: The plan pattern of snow echoes at the generating level. *J. Meteor.*, **13**, 554–560.

Marshall, J. S., 1953: Precipitation trajectories and patterns. *J. Meteor.*, **10**, 25–29.

Oddie, B., 1959: Some cirrus cloud observations made by the Westminister Shiant Isles expedition. *Weather*, **4**, 204–208.

Wexler, R., 1955: Radar analysis of precipitation streamers observed 25 February 1954. *J. Meteor.*, **12**, 391–393.

——, and D. Atlas, 1959: Precipitation generating cells. *J. Meteor.*, **16**, 327–332.

Yagi, T., 1969: On the relation between the shape of cirrus clouds and the static stability of the cloud level—Studies of cirrus clouds. Part IV. *J. Meteor. Soc. Japan*, Ser. II, **47**, 59–64.